Effects of Dynamics and Environment on ^{15}N Chemical Shielding Anisotropy in Proteins. A Combination of Density Functional Theory, Molecular Dynamics Simulation, and NMR Relaxation

C. Scheurer,[†] N. R. Skrynnikov,[†] S. F. Lienin,[†] S. K. Straus,[†] R. Brüschweiler,*[,†,‡,§] and R. R. Ernst*[,†,||]

Contribution from the Laboratorium für Physikalische Chemie, ETH Zentrum, 8092 Zürich, Switzerland, and Carlson School of Chemistry, Clark University, Worcester, Massachusetts 01610

Received December 2, 1998

Abstract: The interpretation of nuclear spin relaxation data of biomolecules often requires the accurate knowledge of chemical shielding anisotropy (CSA) tensors, which significantly depend on the environment and on intramolecular dynamics. CSA tensors are studied in this work by density functional theory and by molecular dynamics simulations. It is demonstrated that density functional theory yields CSA tensors for ^{15}N nuclei in the side chain of crystalline asparagine and in the peptide bond of crystalline alanine−alanine dipeptide with an accuracy comparable to that of solid-state NMR. In these calculations, the molecular fragment containing the nucleus of interest is treated with an IGLO-II and IGLO-III basis set while neighboring fragments exhibiting close contacts are represented by a DZVP set. In addition, electrostatic effects are taken into account by explicit partial point charges. The dynamical averaging of CSA tensors is investigated by applying density functional theory to snapshots of a molecular dynamics trajectory of the protein ubiquitin. The fluctuation properties of the ^{15}N CSA tensors of two glutamine side chains are assessed. Computed auto- and cross-correlated relaxation parameters using these CSA tensors are found to be in good agreement with the experiment. Local charges and close contacts can have a significant effect on ^{15}N CSA tensors and have to be taken into account when transferring CSA parameters from model compounds to proteins.

1. Introduction

The quantitative knowledge of chemical shielding anisotropy (CSA) tensors is important in the context of biomolecular applications of nuclear magnetic resonance (NMR). CSA tensors provide important information on the orientation of molecular fragments and on the electronic environment of the nuclei, which depends on the molecular geometry. Likewise, the CSA contribution to spin relaxation in liquids reflects the overall motion and gives insight into anisotropic intramolecular dynamics.[1] For example, dipole−CSA cross-correlation relaxation experiments probe the correlated modulation of CSA and magnetic dipole interactions.[2] Because the fitting of motional models using such data strongly depends on the choice of CSA tensors, a quantitative interpretation of experimental data can greatly benefit from an accurate knowledge of CSA tensors obtained from other sources.

Recent progress in quantum chemical methods for the calculation of CSA tensors allows applications to biological molecules of moderate size with increasingly quantitative agreement with experimental data.[3−7] The inclusion of electron correlation effects turned out to be crucial for improving the accuracy of calculated CSA tensors. Post-Hartree−Fock (post-HF) methods[8] accounting for electron correlation are computationally expensive and they are mainly applied to relatively small or highly symmetric molecules. The computation time of the fastest conventional post-HF method, MP2, scales as $O(N^5)$ with the number N of electron basis functions. Over recent years, alternative methods based on density functional theory (DFT)[9,10] have been developed. These methods implicitly include electron correlation effects and the computational costs scale as $O(N^3)$. DFT methods for calculating CSA tensors[11] are therefore also applicable to larger molecules and they have proven to be particularly useful for the treatment of model systems that represent essential fragments of larger biomolecules. *N*-Methylacetamide (NMA), for example, is often used as a substitute for the peptide bond moiety. Despite its relatively small size, NMA has allowed one to gain valuable insight into the origins of the chemical

[†] ETH Zentrum.
[‡] Clark University.
[§] Corresponding author: (phone) (508) 793-7220; (fax) (508) 793-8861; (e-mail) rbruschw@nmr.clarku.edu.
[||] Corresponding author: (phone) +41 1 632 43 68; (fax) +41 1 632 12 57; (e-mail) ernst@nmr.phys.chem.ethz.ch.

(1) (a) Bremi, T.; Brüschweiler, R. *J. Am. Chem. Soc.* **1997**, *119*, 6672−6673. (b) Lienin, S. F.; Bremi, T.; Brutscher, B.; Brüschweiler, R.; Ernst, R. R. *J. Am. Chem. Soc.* **1998**, *120*, 9870−9879.
(2) (a) Tjandra, A.; Szabo, A.; Bax, A. *J. Am. Chem. Soc.* **1996**, *118*, 6986−6991. (b) Brutscher, B.; Skrynnikov, N. R.; Bremi, T.; Brüschweiler, R.; Ernst, R. R. *J. Magn. Reson.* **1998**, *130*, 346−351. (c) Yang, D. W.; Konrat, R.; Kay, L. E. *J. Am. Chem. Soc.* **1997**, *119*, 11938−11940. (d) Yang, D. W.; Gardner, K. H.; Kay, L. E. *J. Biomol. NMR* **1998**, *11*, 213−220.
(3) deDios, A. C.; Pearson, J. G.; Oldfield, E. *Science* **1993**, *260*, 1491−1496.
(4) (a) Le, H.; Pearson, J. G.; de Dios, A. C.; Oldfield, E. *J. Am. Chem. Soc.* **1995**, *117*, 3800−3807. (b) Malkin, V. G.; Malkina, O. L.; Salahub, D. R. *J. Am. Chem. Soc.* **1995**, *117*, 3294−3295.
(5) de Dios, A. C. *Prog. NMR Spectrosc.* **1996**, *29*, 229−278.
(6) Sitkoff, D.; Case, D. A. *J. Am. Chem. Soc.* **1997**, *119*, 12262−12273.
(7) Sitkoff, D.; Case, D. A. *Prog. NMR Spectrosc.* **1998**, *32*, 165−190.
(8) Szabo, A.; Ostlund, N. S. *Modern Quantum Chemistry: Introduction to Advanced Electronic Structure Theory*; McGraw-Hill: New York, 1989.
(9) Hohenberg, P.; Kohn, W. *Phys. Rev. B* **1964**, *136*, 864−871. Kohn, W.; Sham, L. J. *Phys. Rev. A* **1965**, *140*, 1133−1138.
(10) Parr, R. G.; Yang W. *Density Functional Theory of Atoms and Molecules*; Oxford University Press: Oxford, 1989.
(11) Malkin, V. G.; Malkina, O. L.; Casida, M. E.; Salahub, D. R. *J. Am. Chem. Soc.* **1994**, *116*, 5898−5908.

10.1021/ja984159b CCC: $18.00
Published on Web 04/17/1999

shielding properties of nuclei within the peptide plane.[7,12] A quantitative interpretation of NMR relaxation data, however, requires a level of accuracy that can only be achieved by treating more extended fragments at higher computational costs.

In the present paper, ^{15}N CSA tensors of biomolecules are calculated by DFT in order to explore their dependence on local structure, dynamics, close nonbonded contacts, and electrostatic effects. For this purpose, it is convenient to divide the major contributions to the CSA tensors into three parts:[3,7] (i) the short-range contributions, which are treated by explicit quantum chemical methods, (ii) the electrostatic contributions, and (iii) the magnetic susceptibility contributions. The short-range contributions can be further divided into covalently bonded interactions and weakly bonded or nonbonded close contacts which, in the case of biomolecules, are mainly due to hydrogen bonds. The electrostatic contributions are treated by explicit partial point charges, which is sometimes referred to as the charge field perturbation (CFP) approach.[3] The magnetic long-range contributions, which may lead to ring-current shifts or, in paramagnetic systems, to pseudocontact shifts, will not be discussed here (for a recent review see ref 7). Only the anisotropic part of the CSA tensors is considered; isotropic chemical shifts will not be discussed.

In section 2, the reliability of the method is assessed for model systems with a well-defined rigid structure and known environment. The ^{15}N CSA tensor of the side-chain amide group of crystalline asparagine and the ^{15}N CSA tensor of the peptide bond of the L-alanyl-L-alanine dipeptide are calculated. The latter provides a model for backbone peptide planes in proteins. The resulting CSA tensors are compared with experimental solid-state NMR data taken from the literature.

In addition, one has to be aware that CSA tensors of flexible molecules are time-dependent quantities. Overall rotational tumbling and intramolecular rigid-body motion of the molecular fragment to which a CSA tensor is attached merely reorient the principal axis system of the CSA tensor. Changes of the internal geometry or the electronic environment, on the other hand, affect the magnitude of the principal values as well as the principal axis directions of the CSA tensor in a molecular frame. Depending on the NMR experiment, the CSA tensor fluctuations are sensed differently. While NMR experiments of molecules in the solid state yield linearly time-averaged CSA tensors, NMR relaxation experiments in solution reflect the variance of CSA tensor fluctuations via second-order perturbation theory. In this paper, the time modulation of CSA tensors is investigated by DFT calculations applied to snapshots of a molecular dynamics (MD) computer simulation of the protein ubiquitin (76 amino acid residues). The calculated time dependence of the ^{15}N CSA tensors is compared with ^{15}N relaxation data of selected glutamine side chains (section 4). A related procedure was applied previously to gramicidin A,[12] where ^{15}N CSA tensors were calculated for selected snapshots of a MD trajectory for comparison with CSA tensors measured by solid-state NMR.

2. Effects of the Environment on CSA Tensors Assessed by DFT Calculations

DFT Procedure. For the chemical shielding calculations, the sum-over-states density functional perturbation theory (SOS-DFPT),[11,13] as implemented in the deMon NMR program,[14−16] was used. In this method, Kohn−Sham orbitals are applied to the Ramsey formula for chemical shielding[17] and the energy denominators are approximated by differences in Kohn−Sham orbital energies, corrected for changes upon excitation in the exchange correlation potential. The shieldings were calculated using the Loc.1 SOS-DFPT approximation,[11] with the molecular orbitals localized by the method of Boys.[18] The gradient-corrected Perdew−Wang-91 (PW91) exchange-correlation potential[19] was used. Numerical quadrature was carried out on FINE RANDOM angular grids[14,16] with 64 radial shells. Calculations were performed using either the IGLO-II or the IGLO-III basis sets.[20] Explicitly included fragments that represent the environment were treated by the less expensive Gaussian orbital basis set DZVP.[21] In section 4, water solvent molecules within a certain cutoff distance were explicitly included.

Selection of Model Compounds. To explore the effect of the molecular environment on the ^{15}N CSA tensors, DFT calculations were performed for two rigid test systems by considering different degrees of inclusion of environmental effects. We have selected the side-chain amide group of crystalline ^{15}N asparagine·H_2O and the peptide bond ^{15}N of the dipeptide L-alanyl-L-alanine (AlaAla). For both systems, X-ray or neutron-diffraction structures and ^{15}N CSA tensors from solid-state NMR studies are reported in the literature. Since the structures of the chosen crystals do not show large-amplitude motions, the CSA tensors could be calculated from the (average) X-ray or neutron-diffraction coordinate sets without additional averaging over internal motional modes. The effect of internal motions on CSA tensors is addressed later in this paper for ubiquitin. While the peptide bond nitrogen of the AlaAla dipeptide represents a model for protein backbone nitrogens, the selection of the asparagine side-chain nitrogen is motivated by the dynamical investigation of the related glutamine side chains presented in section 3.

Asparagine Side-Chain Nitrogen. Judging from the crystal structure,[22] Asn·H_2O is well suited for testing quantum-chemical methods: the crystal water molecules occupy well-defined positions, and the coordinates of the H-atoms are known with high accuracy from neutron-scattering experiments. Based on the coordinate set from ref 22a, the factors determining the ^{15}N side-chain CSA tensor were decomposed into close-contact and charge-field contributions, as mentioned in the Introduction. The hydrogen-bond partners to C═O and N−H in the amide group were considered as close contacts. As indicated in Figure 1, these are the atoms N2−H7···O2, N2−H6···O1, and O3···H5−N1, where the H-bond partners are symmetrically equivalent neighbor Asn molecules (for details see Supporting Information). The COO^- contacts are accounted for by acetate substitutes

(12) Woolf, T. B.; Malkin, V. G.; Malkina, O. L.; Salahub, D. R.; Roux, B. *Chem. Phys. Lett.* **1995**, *239*, 186−194.

(13) Malkin, V. G.; Malkina, O. L.; Eriksson, L. A.; Salahub, D. R. In *Modern Density Functional Theory: A Tool for Chemists*; Seminario, J. M., Politzer, P., Eds.; Elsevier: Amsterdam, 1995; Vol. 2, p 273.

(14) Malkin, V. G.; Malkina, O. L.; Salahub, D. R. *Chem. Phys. Lett.* **1996**, *261*, 335−345.

(15) Salahub, D. R.; Fournier, R.; Mlynarski, P.; Papai, I.; St-Amant, A.; Ushio, J. In *Density Functional Methods in Chemistry*; Labanowski, A., Andzelm, J., Eds.; Springer: New York, 1991; p 77.

(16) St-Amant, A.; Salahub, D. R. *Chem. Phys. Lett.* **1990**, *169*, 387−392.

(17) Ramsey, N. F. *Phys. Rev.* **1950**, *78*, 699−703.

(18) Foster, S.; Boys, S. *Rev. Mod. Phys.* **1960**, *32*, 303−304.

(19) Perdew, J. P.; Wang, Y. *Phys. Rev. B* **1992**, *45*, 13244−13249.

(20) Kutzelnigg, W.; Fleischer, U.; Schindler, M. In *NMR: Basic Principles and Progress*; Diehl, P., Fluck, E., Kosfeld, E., Eds.; Springer: Berlin, 1991; Vol. 23, pp 165−262.

(21) (a) Godbout, N.; Salahub, D. R.; Andzelm, J.; Wimmer, E. *Can. J. Chem.* **1992**, *70*, 560−571. (b) Sosa, C.; Andzelm, J.; Elkin, B. C.; Wimmer, E.; Dobbs, K. D.; Dixon, D. A. *J. Phys. Chem.* **1992**, *96*, 6630−6636

(22) (a) Verbist, J. J.; Lehmann, M. S.; Koetzle, T. F.; Hamilton, W. C. *Acta Crystallogr.* **1972**, *B28*, 3006−3013. (b) Ramanadham, M.; Sikka, S. K., Chidambaram, R. *Acta Crystallogr.* **1972**, *B28*, 3000−3005.

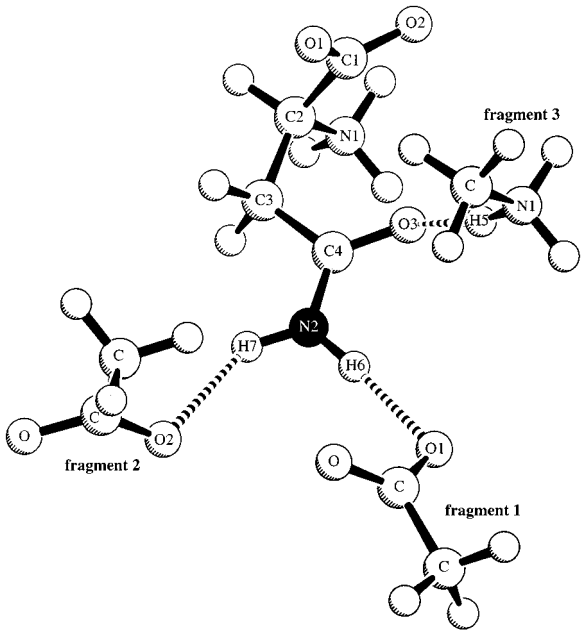

Figure 1. Molecular model used for the DFT calculation of the chemical shielding tensor of ^{15}N2 in crystalline Asn·H_2O. The hydrogen bonds in crystalline Asn·H_2O are represented by interactions to acetate and protonated methylamine ions acting as small substitutes.

(fragments 1 and 2), while the NH_3^+ group is mimicked by a protonated methylamine (fragment 3). The geometric arrangement as well as the numbering scheme are given in Figure 1. For these substitutes, the smaller DZVP basis set was used.

Since asparagine crystallizes in its zwitterionic form, special attention needs to be paid to short-range electrostatic effects. These were modeled by point charges located on all partially charged atoms that lie within a certain cutoff radius. The cutoff radius is defined by the distances between the N- and O-atoms in the amide group and those in neighboring molecules. The charges were taken from the molecular dynamics program GROMOS96:[23] for COO^- from a model aspartic acid side chain, for NH_3^+ from a model lysine side chain, and for water from the SPC model. For the asparagine NH_3^+ group, the partial charge of the C^ϵ atom was added to the nitrogen partial charge.

The amide ^{15}N CSA tensors were calculated for the combination of PW91 exchange-correlation functional with the IGLO-II basis set and for several different treatments of the environment. Results illustrating the trends found in the calculations are summarized in Table 1, which also contains the CSA tensor values determined experimentally by solid-state NMR.[24] A comparison of rows b and e in Table 1 shows that electrostatic effects of the environment are important, as expected. Inclusion of point charges within a 3.2- or 10-Å cutoff radius, yielding zero net charges inside these surfaces, gives nearly quantitative agreement with the experimental CSA principal values. Similarly accurate values for the CSA principal values are obtained when, in addition to point charges, the computations include neighboring fragments that form hydrogen bonds to Asn and that are treated explicitly using the DZVP basis set (row e). However, a systematic difference is found for the principal axis directions as compared to a treatment that takes into account the environment by point charges only (rows c and d). A more detailed analysis shows that this effect is caused mainly by fragment 1, which exhibits the strongest hydrogen bond to the amide plane protons (see Figure 1 and Table 1, rows e and f) with an N2−H6−O1 angle of 173.3° and a distance N2−O1 of 2.927 Å. Fragment 3 forms a hydrogen bond N1−H5−O3 to the more remote O3 atom with a distance N1−O3 of 2.806 Å. The larger deviation of the corresponding hydrogen bond angle of 168.1° from linearity leads to a smaller effect on the ^{15}N CSA tensor. Unfortunately, a quantitative comparison of the computed axis directions (expressed by the angles α and β) with experimental values is not possible since the experimental angles were not determined with sufficient accuracy. In section 4, liquid-state NMR relaxation data are presented for glutamine side chains in ubiquitin that lend experimental support to the CSA orientations obtained from the DFT calculations.

An accurate CSA tensor can be computed at lower computational costs when only fragment 1 is treated explicitly and fragments 2 and 3 are represented, together with the remaining surroundings, by point charges within a 10-Å cutoff distance (Table 1, row f). A further speedup can be achieved by the use of locally dense basis sets.[25] In this case, the carboxamide group of Asn and C^β are treated with the IGLO-II basis set while the other Asn atoms are represented, together with fragment 1, by the DZVP basis set (Table 1, row g).

The explicit quantum-chemical treatment of fragments that participate in strong hydrogen bonds with the amide bond and a partial charge representation of the remaining environment provides a computationally efficient method for accurate ^{15}N CSA calculations.

A comprehensive treatment of the entire environment within a 3.2-Å cutoff (including besides fragments 1−3, molecular fragments that do not form hydrogen bonds) by a DZVD basis set requiring more than 800 basis functions was also carried out. Although it is computionally much more expensive, it produced substantially poorer results, presumably because it involves vacuum electrostatic boundary conditions along the cutoff surface. These results indicate that the electrostatic situation is modeled more realistically by partial point charges which are adapted to reflect the effect of a condensed environment.

We also tested whether the use of the larger IGLO-III basis set for the amide group and for C^β would lead to a further improvement. Some of the calculations described above were repeated with this basis set, but no systematic improvement was found. To further improve accuracy, it is likely that magnetic susceptibility effects would need to be taken into account.

AlaAla Peptide Bond Nitrogen. A procedure similar to that for Asn was applied for the ^{15}N CSA tensor of the peptide bond in the dipeptide L-Ala-L-Ala. In contrast to Asn, no neutron-scattering coordinates are available for the hydrogen positions. Moreover, in the X-ray structure,[26] one methyl hydrogen is missing and the other methyl hydrogens and the amine group show rather uncommon bond lengths and angles. To improve the geometry, the missing hydrogen was added and the structure energy-minimized using the CHARMM force field[27] while keeping the heavy atoms as well as the orientation of the amine

(23) van Gunsteren, W. F.; Billeter, S. R.; Eising, A. A.; Hünenberger, P. H.; Krüger, P.; Mark, A. E.; Scott, W. R. P.; Tironi, I. G. *Biomolecular Simulation: The GROMOS96 Manual and User Guide*; Biomos b.v.: Zürich, Groningen, 1996.

(24) Herzfeld, J.; Roberts, J. E.; Griffin, R. G. *J. Chem. Phys*. **1987**, *86*, 597−602.

(25) Chesnut, D. B.; Moore, K. D. *J. Comput. Chem*. **1989**, *10*, 648−659.

(26) Fletterick, F.; Tsai, C.; Hughes, R. E. *J. Phys. Chem.* **1971**, *75*, 918−922.

(27) MacKerell, A. D., Jr.; Bashford, D.; Bellott, M.; Dunbrack, R. L., Jr.; Evanseck, J. D.; Field, M. J.; Fischer, S.; Gao, J.; Guo, H.; Ha, S.; Joseph-McCarthy, D.; Kuchnir, L.; Kuczera, K.; Lau, F. T. K.; Mattos, C.; Michnick, S.; Ngo, T.; Nguyen, D. T.; Prodhom, B.; Reiher, W. E., III; Roux, B.; Schlenkrich, M.; Smith, J. C.; Stote, R.; Straub, J.; Watanabe, M.; Wiorkiewicz-Kuczera, J.; Yin, D.; Karplus, M. *J. Phys. Chem. B* **1998**, *102*, 3586−3616.

Table 1. Comparison of Experimental Results and DFT Calculations for the ^{15}N CSA Tensor of Asparagine[a]

	neighboring fragments included	cutoff radius for point charges (Å)	σ_{xx}[b] (ppm)	σ_{yy}[b] (ppm)	σ_{zz}[b] (ppm)	η[c]	α[d] (deg)	β[d] (deg)
a		no pt charges	77.59	12.08	−89.67	0.731	9.88	2.69
b	1, 2, 3	no pt charges	75.08	58.50	−133.58	0.124	18.53	14.99
c		3.2	76.64	34.55	−111.19	0.378	10.06	2.79
d		10	76.95	31.92	−108.87	0.414	9.88	2.12
e	1, 2, 3	10	75.22	36.60	−111.82	0.345	13.78	8.92
f	1	10	76.95	33.75	−110.70	0.390	13.18	4.33
g	1	10	76.73	33.26	−109.99	0.395	13.06	4.38
solid-state NMR expt[24]			76.5	33.1	−109.6	0.396	0.00[d]	0.00[d]

[a] In all calculations the atoms belonging to the amide group and the neighboring aliphatic carbon were treated with the IGLO-II basis set and the H-bonded fragments with DZVP functions. In calculations a−f, the rest of the Asn molecule was also equipped with IGLO-II basis functions, while in calculation g, DZVP functions were used instead. [b] Principal values of trace-free part of the ^{15}N CSA tensor. [c] Asymmetry η of CSA tensor defined by $\eta = (\sigma_{yy} - \sigma_{xx})/\sigma_{zz}$. [d] The angle α is defined as the angle between the x principal axis of the CSA tensor and the amide C−N bond while β is the angle between the y principal axis and the normal to the carboxamide plane. In ref 24, $\alpha = \beta = 0°$ was assumed for the interpretation of the solid-state NMR measurements.

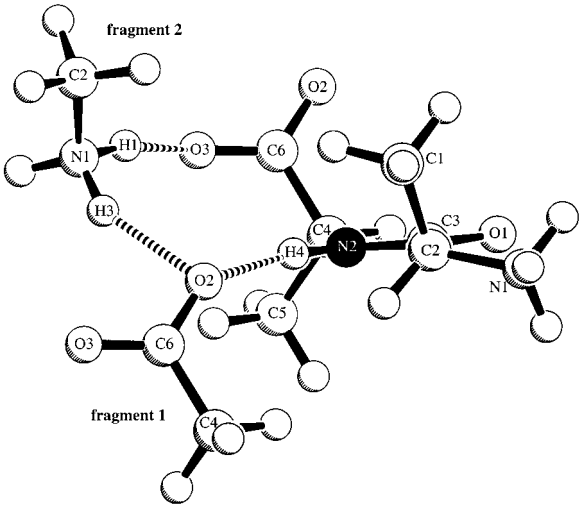

Figure 2. Molecular model used for DFT calculation of the chemical shielding tensor of $^{15}N2$ in crystalline AlaAla. The hydrogen-bonding network in crystalline AlaAla is represented by interactions with acetate and methylamine ions acting as small substitutes.

group fixed (for details see Supporting Information). As noted in the X-ray study,[28] the carbonyl oxygen O1 in the peptide plane is not hydrogen-bonded and the only close contacts are intrapeptide contacts to the protons of N1 (see Figure 2). Therefore, the only close contact affecting N2 is the hydrogen bond N2−H4···O2. To account for the intermolecular hydrogen bonding, an acetate and a protonated methylamine dummy ion were introduced (Figure 2).

Calculations on a single AlaAla molecule with and without the two hydrogen-bonded fragments are given in Table 2 (rows a and b). It also contains the CSA tensor determined experimentally by solid-state NMR.[28] Inclusion of the environment in the form of partial charges within a cutoff distance of 13 Å around the peptide plane yields good agreement with the experimental values (Table 2, row c). It is important to choose the cutoff distance such that the net charge inside the cutoff region is zero. As for Asn, the reduction of the basis set size to DZVP for all atoms not directly connected to the peptide plane does not significantly decrease the accuracy of the CSA tensors (Table 2, row d). The deviation between calculated and experimental values, which is somewhat larger than for Asn·H_2O, may be caused in part by the aforementioned uncertainties of the X-ray structure. The effects of nonideal geometries were also found to be important for ^{15}N CSA tensors of nucleic acids.[29]

The orientations of the CSA principal axes agree well with the experiment (see Table 2). In particular, the assumption made in the solid-state NMR analysis that the z axis lies in the peptide plane, exhibiting an angle of 106° with the N−C bond, is confirmed by the calculations. While fragment 2 does not form hydrogen bonds to atoms in the close vicinity of the N2 atom, the two hydrogen bonds that are formed, closing a circle of a hydrogen-bonding network (Figure 2), still have a noticeable influence on the ^{15}N CSA tensor.

3. Dynamical Averaging of CSA Tensors by Intramolecular Motion in Proteins

Chemical shielding tensors, having their origin in the electronic molecular configuration, are quite sensitive to changes in molecular geometry. The CSA tensors of a flexible molecule are thus time-dependent regarding their principal values and the orientations of the principal axes. The extent of dynamical modulation of CSA tensors shall be investigated in this section based on a molecular dynamics simulation trajectory of the protein ubiquitin. The values obtained are then used in section 4 to analyze dipole−CSA cross-correlated relaxation measurements.

Strategy for CSA DFT Calculations in Proteins. The calculation of time-averaged CSA tensors in proteins starts with the recording of an extended molecular dynamics simulation trajectory from which a representative number of frames is selected. For each frame, the CSA parameters are then computed by a DFT procedure following the approach indicated in the previous chapter.

Because it is impossible to perform a DFT calculation on an entire protein, an appropriate model fragment is selected that contains the nucleus (or nuclei) for which the CSA tensor is calculated, with a bonding topology that mimics the original environment and that is, at the same time, small enough to be treated by DFT. The IGLO-II or IGLO-III basis sets are used for the atoms of interest and for all neighboring atoms belonging to this fragment. If the atom for which a CSA tensor is calculated is part of a delocalized electron system, such as an amide plane or an aromatic ring system, all atoms in this system as well as their nearest neighbors are treated by the IGLO basis. For all other atoms, a DZVP basis set is used. In a second step, the close contacts are identified. In biomolecules, these are mainly "strong" hydrogen bonds that involve the atom(s) of interest or one of its neighbors. A typical hydrogen bond of the type C═O...H−N can be considered as "strong" if the distance between the heavy atoms O and N is below 3.2 Å and if the angle

(28) Hartzell, C. J.; Whitfield, M.; Oas, T. G.; Drobny, G. P. *J. Am. Chem. Soc.* **1987**, *109*, 5966−5969.

(29) Hu, J. Z.; Facelli, J. C.; Alderman, D. W.; Pugmire, R. J.; Grant, D. M. *J. Am. Chem. Soc.* **1998**, *120*, 9863−9869.

Table 2. Comparison of Experimental Results and DFT Calculations for the ^{15}N CSA Tensor of the Peptide Bond in AlaAla[a]

	neighboring fragments included	cutoff radius for point charges (Å)	σ_{xx} (ppm)	σ_{yy} (ppm)	σ_{zz} (ppm)	$\Delta\sigma$[b] (ppm)	η	β[c] (deg)
a		no pt charges	61.00	53.00	−114.10	−171.12	0.069	105.7
b	1, 2	no pt charges	61.11	50.29	−111.40	−167.10	0.097	108.2
c	1, 2	13	56.47	42.87	−99.34	−149.01	0.137	105.9
d	1, 2	13	56.98	41.97	−98.95	−148.43	0.152	105.8
solid-state NMR expt[28]			54.3	41.6	−95.9	−144	0.133	106

[a] In all calculations, the atoms belonging to the peptide plane and the neighboring C^α atoms were treated with the IGLO-II basis set and the H-bonded fragments with DZVP functions. In calculations a−c also the rest of the AlaAla molecule was equipped with IGLO-II basis functions, while in calculation d, DZVP functions were used instead. [b] $\Delta\sigma \equiv 3\sigma_{zz}/2$. [c] β is the angle between the z principal axis and the N−C′ bond. For the interpretation of the experimental results, the z axis was assumed to lie in the amide plane.[28]

N−H−O is near 180°. The close contacts may influence both the anisotropy and orientation of the CSA tensor. The contact partners are then substituted by small molecules. In particular, carboxylic acids are replaced by acetate molecules, amino groups by methylamines, and peptide planes by NMA or acetamides. Closeby water molecules and other small fragments are treated using the DZVP basis set. In a third and final step, the partial charge distribution of the environment is included. Its effect is particularly important in the presence of surrounding fragments that carry net charges, such as deprotonated carboxyl or protonated amino groups. To take this effect into account, a 10−15-Å cutoff distance for the surrounding, which should be chosen such that the total charge inside this surface is zero, appears to be sufficient.

Molecular Dynamics Trajectory of Ubiquitin. For the investigation of the time modulation of side-chain and backbone ^{15}N CSA tensors, a molecular dynamics trajectory of the small globular protein ubiquitin with 76 amino acid residues was computed by the program CHARMM 24.[30] The protein structure has been well characterized by X-ray crystallography[31] and by NMR spectroscopy.[1b,32−34] From the 2.5-ns MD trajectory of ubiquitin at 300 K in a cubic box containing 2909 explicit water molecules, 625 snapshots with a time increment of 4 ps have been selected for further analysis. Details of the simulation and results of the first 1.5 ns of the trajectory were described previously.[1b] In the following, we analyze the dynamical effects on the ^{15}N CSA tensors of the glutamine side chains whose structure and properties are similar to the ones of asparagine. The effects on the main-chain ^{15}N CSA tensors will be presented elsewhere.

Glutamine Side-Chain Dynamics in Ubiquitin. Human ubiquitin contains six glutamine (Gln) residues. The Gln side chains constitute important elements in proteins because of their dual role as electron donors (amino group) and acceptors (carbonyl). For example, the presence of these side chains in various proteins is important for their conjugation to ubiquitin.[35]

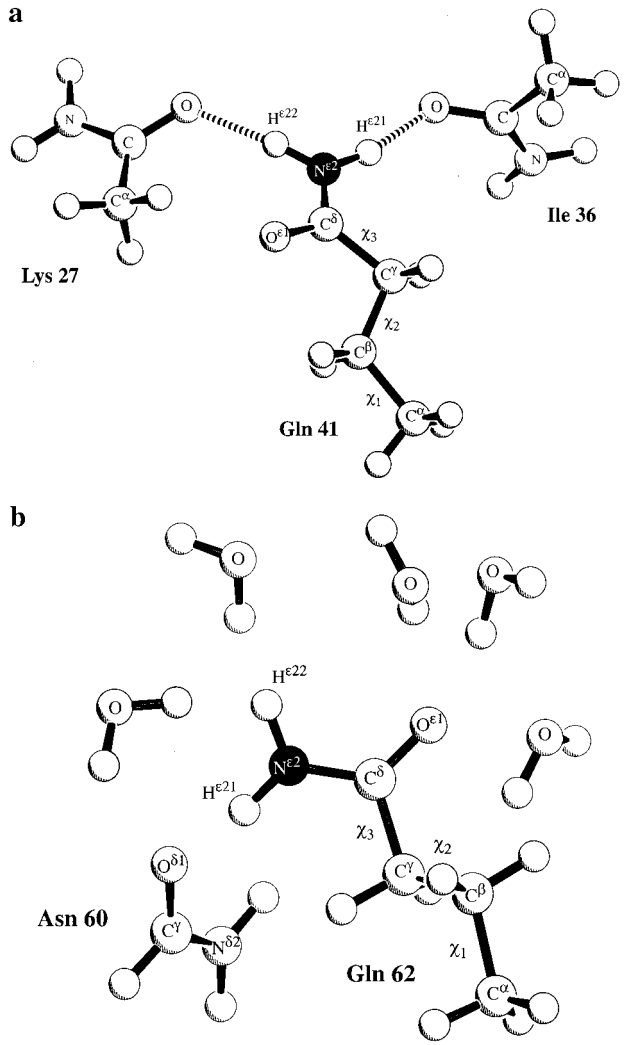

Figure 3. Typical snapshots based on an MD trajectory of ubiquitin and used for the DFT computation of the side-chain $^{15}N^{\epsilon 2}$ CSA tensors for (a) Gln 41 and (b) Gln 62. The intramolecular hydrogen-bonding partners are represented by acetamide and formamide molecules as small substitutes.

The Gln side chain is shown in Figure 3 where the dihedral angles χ_1, χ_2, and χ_3 are also indicated (χ_3 is defined by the four atoms $C^\beta-C^\gamma-C^\delta-O^{\epsilon 1}$ [36]). The carboxamide group, $C^\gamma-C(=O)-NH_2$, has on average a planar structure subject to small dynamic distortions. In terms of orbital hybridization and bonding, it is similar to a backbone peptide plane fragment. The motion exhibited by the carboxamide groups was examined on the basis of the MD trajectory. The relaxation-active motional modes were characterized by computing model correlation

(30) Brooks, R. B.; Bruccoleri, R. E.; Olafson, B. D.; States, D. J.; Swaminathan, S.; Karplus, M. *J. Comput. Chem.* **1983**, *4*, 187.
(31) Vijay-Kumar, S.; Bugg, C. E.; Cook, W. J. *J. Mol. Biol.* **1987**, *194*, 531−544.
(32) Di Stefano, D. L.; Wand, A. J. *Biochemistry* **1987**, *26*, 7272−7281. Weber, P. L.; Brown, S. C., Mueller, L. *Biochemistry* **1987**, *26*, 7282−7290.
(33) Schneider, D. M.; Dellwo, M. J.; Wand, A. J. *Biochemistry* **1992**, *31*, 3645−3652. Wand, A. J.; Urbauer, J. L.; McEvoy, R. P.; Bieber, R. J. *Biochemistry* **1996**, *35*, 6116−6125.
(34) (a) Tjandra, N.; Feller, S. E.; Pastor, R. W.; Bax, A. *J. Am. Chem. Soc.* **1995**, *117*, 12562−12566. (b) Wang, A. C.; Grzesiek, S.; Tschudin, R.; Lodi, P. J.; Bax, A. *J. Biomol. NMR* **1995**, *5*, 376−382. (c) Tjandra, N.; Szabo A.; Bax, A. *J. Am. Chem. Soc.* **1996**, *118*, 6264−6272. (d) Ottiger, M.; Tjandra, N.; Bax, A. *J. Am. Chem. Soc.* **1997**, *119*, 9825−9830.
(35) King, R. W.; Glotzer, M.; Kirschner, M. W. *Mol. Biol. Cell* **1996**, *7*, 1343−1357. Grigoryev, S.; Stewart, A. E.; Kwon, Y. T.; Arfin, S. M.; Bradshaw, R. A.; Jenkins, N. A.; Copeland, N. G.; Varshavsky, A. *J. Biol. Chem.* **1996**, *271*, 28521−28532.
(36) McIntosh, L. P.; Brun, E.; Kay, L. E. *J. Biomol. NMR* **1997**, *9*, 306−312.

functions limited to some specific degrees of freedom, such as $\chi_1(t)$, $\chi_2(t)$, and $\chi_3(t)$, similar to the procedure described in ref 37. It is found that the following forms of internal motion can be relevant for spin relaxation in Gln carboxamide groups: (i) rapid wagging/twisting motion of the $N^{\epsilon 2}H^{\epsilon 21}$ and $N^{\epsilon 2}H^{\epsilon 22}$ vectors. (ii) Rotation about the dihedral angles χ_1, χ_2, and χ_3. For χ_1 and χ_2, rotation is determined by a standard 3-fold staggered internal potential. For the $\chi_2 = 180°$ rotamer, rotation about χ_3 occurs rather freely (an internal energy barrier of 8 kJ/mol was found in our DFT computations), unless it is constrained by the more distant environment, such as for Gln 41, where the constrained geometry leads to a significant amount of anticorrelation between the rotations about χ_1 and χ_3. (iii) Slow time scale backbone dynamics accompanied by reorientations of the $C^{\alpha}-C^{\beta}$ vectors with respect to the overall diffusion frame of reference.

In reality, chemical-exchange processes involving the $H^{\epsilon 2}$ protons do also take place, which are not displayed by the MD simulation protocol. Exchange can either occur with water protons or in form of hindered rotation about the $C^{\delta}-N^{\epsilon 2}$ bond.[38] These processes are too slow to directly induce spin relaxation, but they can influence the experimental results by partially averaging the relaxation parameters involving the $H^{\epsilon 21}$ and $H^{\epsilon 22}$ protons (vide infra).

Among all Gln side chains of ubiquitin, Gln 41 is the one that is most rigidly locked in the core of the protein. The other Gln side chains are to a variable extent exposed to the solvent, exhibiting considerable flexibility. In particular, the side chain of Gln 62 protrudes into the solvent with only little interactions with other parts of the protein. While the motion of the carboxamide group in Gln 62 is dominated by fast rotation about χ_3, in Gln 41 this form of motion is mostly reduced to low-amplitude axial fluctuations. The two extreme behaviors displayed by Gln 41 and Gln 62 are discussed in more detail in the following.

The relaxation behavior of the $^{15}N^{\epsilon 2}$ spin and other spins has been the subject of several studies, which found a good correlation between side-chain mobility and autorelaxation parameters.[39] Here we focus on the $^{15}N^{\epsilon 2}$ CSA tensor and its role in dipole−CSA cross-correlated relaxation.

DFT Computations from MD Snapshots. In preparation of the DFT computations, the 625 MD snapshots were aligned by individual rotations that were determined by a mass-weighted least-squares difference criterion considering all protein atoms with respect to a reference snapshot at 250-ps simulation time. The same rotation was applied also to the solvent water molecules. In this way, overall rotational diffusion, which occurs during the simulation, was eliminated yielding atomic coordinates for each snapshot in the same molecular diffusion frame.

At first, DFT computations were carried out on the isolated side chains. For this purpose, the side chains of Gln 41 and Gln 62 from the CHARMM output files were terminated toward the backbone by placing a methyl group at the C^{α} position; i.e., the backbone N and C′ atoms were replaced by protons and the lengths of the new C−H bonds were set to 1.09 Å. The ^{15}N CSA tensors were then calculated using deMon with the IGLO-III basis set for all atoms. This procedure was applied to all 625 snapshots and the resulting CSA tensors were stored as a "CSA trajectory", where each snapshot contains the full CSA tensors expressed in the (reoriented) coordinate frame of the CHARMM coordinate files.

In a next stage, environmental effects were taken into account. Inspection of the MD trajectory showed that the Gln 62 carboxamide group comes in close contact with water molecules and with the side chain of Asn 60, leading to $H^{\epsilon 21}$(Gln)−$O^{\delta 1}$(Asn) and, infrequently, $O^{\epsilon 1}$(Gln)−$H^{\delta 22}$(Asn) contacts. Following the method described in section 2, water molecules were included in the DFT computation explicitly, whereas the Asn 60 moiety was substituted by a formamide molecule. Water or formamide molecules were included in the computations if at least one of their atoms was found within 3.1 Å from $N^{\epsilon 2}$ or $O^{\epsilon 1}$ of Gln 62 (see Figure 3b). DeMon input coordinate sets generated in this way contained on average four to five water molecules. The formamide molecule appears on average in one out of five snapshots. Water and formamide molecules were represented by DZVP basis sets.

Using a similar procedure, CSA trajectories with and without environment were generated for Gln 41. Most of the atoms falling within a range of 3.1 Å from $N^{\epsilon 2}$ or $O^{\epsilon 1}$ of Gln 41 belong to the CH_2 or CH_3 groups of neighboring side chains. Since they have only a small effect on the CSA tensors of interest, they were not included in the DFT computations. However, Gln 41 amino protons, $H^{\epsilon 22}$ and $H^{\epsilon 21}$, form two stable hydrogen bonds with the backbone carbonyl oxygens of Lys 27 and Ile 36, respectively. In an initial set of computations, the backbone fragments Lys 27−Ala 28 and Ile 36−Pro 37 were modeled by NMA and *N*-dimethylacetamide (DNMA) molecules, respectively. In subsequent computations, these fragments were replaced by two acetamide molecules. Since the CSA tensors obtained by the two sets of computations differ for $^{15}N^{\epsilon 2}$ CSA principal values by less than 1 ppm and for the orientations of the principal axes by less than 1°, acetamide molecules were used throughout the final series of computations. Thus, each of the deMon input coordinate files included two acetamides that were treated with the DZVP basis set. The effect of the aromatic groups of phenylalanines and tyrosine located at a distance exceeding 15 Å was neglected.

The $N^{\epsilon 2}$ CSA trajectories of Gln 41 and 62 were analyzed as follows. The traceless parts of the CSA tensors of each snapshot were selected, and the symmetric and antisymmetric parts were separated. The symmetric part, σ^{sym}, was diagonalized yielding the CSA principal values σ_{ii} ($i = x, y, z$) as eigenvalues and the principal axes as eigenvectors. Average σ_{ii}^{sym} values, standard deviations, and average principal axis orientations of σ^{sym} with respect to the local frame of reference are given in Table 3.

The trajectories of CSA principal values display fast fluctuations with a distribution that is in a good approximation Gaussian. The principal axis orientations also undergo fast fluctuations with respect to local chemical bonds. The orientational distributions on the surface of the unit sphere are shown by scatterplots in Figure 4. Slightly narrower orientational distributions are found for the trajectories calculated without taking into account the environment. It can be seen that the *x* and *z* principal axes show out-of-plane excursions which reflect the distortions of the amide plane by similar fast out-of-plane motions of $H^{\epsilon 21}$ and $H^{\epsilon 22}$.

Table 3 displays the average CSA parameters extracted from the trajectories. In agreement with the control calculations for crystalline Asn described in the previous section, the average CSA principal values change markedly when the environment

(37) Bremi, T.; Brüschweiler, R.; Ernst, R. R. *J. Am. Chem. Soc.* **1997**, *119*, 4272−4284.

(38) Redfield, A. G.; Waelder, S. *J. Am. Chem. Soc.* **1979**, *101*, 6151−6162. Tropp, J.; Redfield, A. G. *J. Am. Chem. Soc.* **1980**, *102*, 534−538. Perrin, C. L.; Johnston, E. R.; Lollo, C. P.; Kobrin, P. A. *J. Am. Chem. Soc.* **1981**, *103*, 4691−4696.

(39) Boyd, J. *J. Magn. Reson., Ser. B* **1995**, *107*, 279−285. Buck, M.; Boyd, J.; Redfield, C.; MacKenzie, D. A.; Jeenes, D. J.; Archer, D. B.; Dobson, C. M. *Biochemistry* **1995**, *34*, 4041−4055. LeMaster, D. M.; Kushlan, D. M. *J. Am. Chem. Soc.* **1996**, *118*, 9255−9264.

Table 3. Average $N^{\epsilon 2}$ CSA Tensors and Their Fluctuations for Gln 41 and Gln 62 in Ubiquitin Calculated from CSA Trajectories

$N^{\epsilon 2}$ CSA tensor	$\sigma_{xx}{}^a$ (ppm)	$\sigma_{yy}{}^a$ (ppm)	$\sigma_{zz}{}^a$ (ppm)	α [ϕ;θ]^b (deg)	β^b (deg)
Gln 41 without environment	88.3 ± 6.6	-2.3 ± 4.2	-86.0 ± 6.1	11.3 [11.1; 87.9]	2.3
Gln 41 with environment	80.6 ± 8.4	15.6 ± 7.0	-96.2 ± 6.8	11.3 [11.1; 88.0]	2.9
Gln 62 without environment	84.7 ± 8.7	4.2 ± 7.3	-88.9 ± 7.3	10.0 [10.0; 89.6]	0.4
Gln 62 with environment	79.4 ± 9.7	20.2 ± 9.5	-99.6 ± 8.8	10.3 [10.3; 89.5]	0.5

[a] Average CSA principal axis values and root-mean-square deviations. [b] Directions of principal axes indicated by angles α and β as in Table 1, and polar angles θ and ϕ are defined with respect to the coordinate frame of Figure 4.

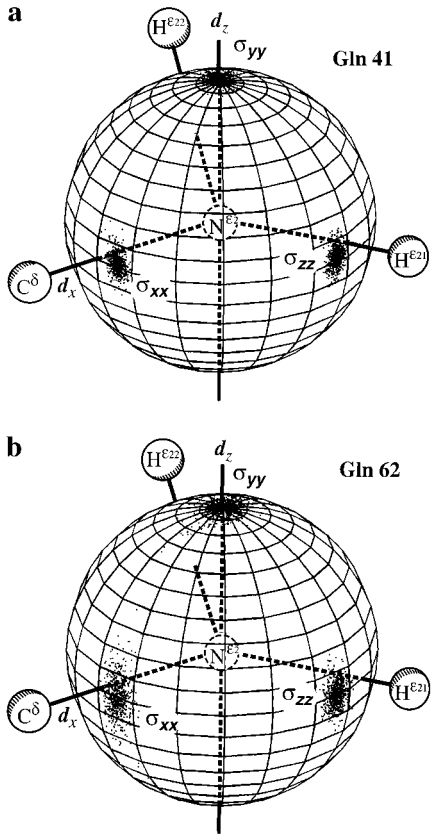

Figure 4. Orientational distribution of the $N^{\epsilon 2}$ CSA tensor (symmetric traceless part) in the coordinate frame of the amide plane calculated by DFT for 625 snapshots of an MD trajectory of ubiquitin taking into account the protein environment for (a) Gln 41 and (b) Gln 62. Each dot on the surface of the unit sphere represents the orientation of the CSA tensor for one of the snapshots. The local frame of reference is defined by the axes d_x along $N^{\epsilon 2}C^{\delta}$, d_z orthogonal to the plane approximately spanned by the atom quartet $N^{\epsilon 2}C^{\delta}H^{\epsilon 21}H^{\epsilon 22}$, and d_y orthogonal to d_x, d_z. The $N^{\epsilon 2}H^{\epsilon 21}$ and $N^{\epsilon 2}H^{\epsilon 22}$ vectors plotted in the graph correspond to their average orientations in the local frame obtained by vector summation over all snapshots.

is explicitly taken into account. The changes are, however, smaller in ubiquitin than for crystalline asparagine, presumably because of the absence of free charges in the close vicinity of the Gln side chains. The average orientations of the CSA principal axes are only slightly affected by the inclusion of the environment for ubiquitin (Table 3), which is in contrast to crystalline Asn.

A statistical analysis of the CSA trajectories revealed correlations between the CSA principal values and the lengths and the linearity of the hydrogen bonds formed by $H^{\epsilon 21}$ and $H^{\epsilon 22}$, but no such correlations were found for the fluctuations of the CSA principal axis orientations. Since the CSA tensors also depend significantly and in a nonadditive way on other dynamic parameters including local bond lengths, bond angles, and torsion angles, the analytical parametrization of the CSA tensors in terms of hydrogen-bonding parameters alone turned out to be ineffective.

Considering the different environments and hydrogen bond partners of Gln 41 and Gln 62, the CSA results are surprisingly similar. Thus, the hydrogen bonds of Gln 41 with the backbone and the hydrogen bonds of Gln 62 with water have on average a similar effect on the ^{15}N CSA tensors. This can be understood by noticing that the hydrogen bonds for the two Gln side chains are far from ideal for most of the MD snapshots: hydrogen bonds with a $N^{\epsilon 2}-H-O$ angle in the range from 170 to 190° and a distance between O and $N^{\epsilon 2}$ less than 3.2 Å are found only in 30% of the snapshots of the Gln 41 trajectory and for a few snapshots in the Gln 62 trajectory. As a result, the net effect of the surrounding is largely limited to its electrostatic contributions. The calculated orientations of the CSA principal axes are notably similar to the ones found for the backbone nitrogen, provided the backbone proton H^N is identified with $H^{\epsilon 21}$.[40]

4. Dipole−CSA Cross-Correlated Relaxation Measurements for Glutamine Side Chains in Ubiquitin

Nuclear spin relaxation measurements are known to be a valuable source of information on structural dynamics of biomolecules. The quantitative interpretation of relaxation data in terms of molecular motion requires the accurate knowledge of the strengths and directions of the relaxation-active interactions. Most commonly longitudinal T_1, transverse T_2, and nuclear Overhauser enhancement (NOE) values are collected reflecting the autocorrelation functions of magnetic dipole−dipole and CSA interactions.[41] Recently, there was a revival of interest in dipole−CSA cross-correlated cross-relaxation experiments in biomolecules.[2] These experiments are complementary to standard autorelaxation measurements, since the cross-correlation rate constants are not, or only little, affected by additional relaxation mechanisms, such as chemical and conformational exchange contributions, spin-rotational relaxation, or relaxation by paramagnetic oxygen, which may compromise the interpretation of dipolar or CSA autorelaxation data. Furthermore, transverse cross-correlation effects are confined to subsystems containing two, three, or four spins, while outside spins have little effect.

It is well-known that cross-correlated relaxation data also carry, in addition to the magnitudes of spin interaction tensors, information on the mutual orientation of their principal axes. Hence, these data are particularly sensitive to intramolecular motion. The investigation of dynamics using such data requires an accurate knowledge of the dipolar and CSA interaction tensors. The information contained in cross-correlated relaxation data on CSA tensors and on molecular motion cannot be unambiguously separated because their contributions are multiplicative. It is necessary to use information from other sources, such as solid-state NMR, MD simulations, or CSA quantum calculations.

(40) Stark, R. E.; Jelinski, L. W.; Ruben, D. J.; Torchia, D. A.; Griffin, R. G. *J. Magn. Reson.* **1983**, *55*, 266−273.
(41) Abragam, A. *Principles of Nuclear Magnetism*; Oxford University Press: Oxford, 1961.

In this context it is interesting to test the transferability of CSA tensors, obtained by solid-state NMR for single amino acids or oligopeptides for the interpretation of liquid-state NMR data of proteins. The effect of solvent water on CSA tensors, the origin and the role of CSA fluctuations, and the contribution of the antisymmetric part of CSA tensors to relaxation should also be assessed.

Experimental Information. Dipole−CSA cross-correlated relaxation rates in $^{15}N^{\epsilon 2}H_2$ and $^{15}N^{\epsilon 2}HD$ groups of Gln 41 and 62 side chains of ubiquitin in 50% H_2O/50% D_2O solution were measured by a 3D version of a constant-time experiment proposed by Tjandra et al.[2a] The pulse sequence is given in the Supporting Information. It starts with the creation of coherence of ^{15}N antiphase with respect to one or both protons. During a cross-relaxation time T, the transfer to in-phase coherence, $^{15}N_xH_z \rightarrow {}^{15}N_x$, is monitored. It is combined in a constant-time manner with the recording of the ^{15}N multiplets during the evolution time t_1. During the second evolution time t_2, ^{15}N chemical shifts are active alone, and finally during t_3, proton coherence is detected.

Each Gln side chain gives rise to four resolved cross-peaks in the 2D (ω_2,ω_3) $^{15}N-^1H$ HSQC-type correlation spectra: two cross-peaks arise from molecules with both sites protonated, i.e., from a $H^{\epsilon 2}H^{\epsilon 21}H^{\epsilon 22}$ group, and two cross-peaks arise from the partially deuterated species, i.e., from $N^{\epsilon 2}H^{\epsilon 21}D^{\epsilon 22}$ and $N^{\epsilon 2}D^{\epsilon 21}H^{\epsilon 22}$ groups. The last two cross-peaks can be used to separately measure the dipole−CSA cross-correlated relaxation rates involving the CSA interaction of $N^{\epsilon 2}$ and the $N^{\epsilon 2}H^{\epsilon 21}$ and $N^{\epsilon 2}H^{\epsilon 22}$ dipolar interactions. Assignment of the four cross-peaks for each Gln residue has been accomplished by a HNCOCA-type experiment[42] which correlates the $N^{\epsilon 2}$ with the $H^{\gamma 1(2)}$ resonances previously assigned by Wand and Weber.[32,33] Stereospecific assignment was performed by the recently reported experiment of McIntosh et al.[36]

The intensities of the multiplet lines in ω_1 are extracted and used for the determination of the cross-correlation rate constants.[43] As usual, the constant-time scheme yields peaks with equal line widths in the ω_1 dimension, such that the magnitudes of the dipole−CSA cross-correlation rates are encoded in the peak intensities. For the $N^{\epsilon 2}H^{\epsilon 21}D^{\epsilon 22}$ and $N^{\epsilon 2}D^{\epsilon 21}H^{\epsilon 22}$ groups, the J_{NH} scalar couplings give rise to doublets in the ω_1 dimension, with the two components corresponding to $N_+ \pm 2N_+H_z$ coherences. For the $N^{\epsilon 2}H^{\epsilon 21}H^{\epsilon 22}$ groups, the J_{NH} scalar couplings produce a quartet pattern in the ω_1 dimension, but only the two outer lines with a separation $2J_{NH}$ are observed. They correspond to the coherences $N_+ \pm 2N_+H_z^{\epsilon 21} \pm 2N_+H_z^{\epsilon 22}\,H_z^{\epsilon 22} + 4N_+H_z^{\epsilon 21}\,H_z^{\epsilon 22}$. The two other near-degenerate lines cancel because the initial coherence is prepared in antiphase.

^{15}N-Labeled ubiquitin was dissolved in a 50% H_2O/50% D_2O solvent at pH 4.7. The measurements were carried out at 600-MHz proton resonance frequency at a temperature of 300 K. Under these conditions, any form of the water-catalyzed exchange is too slow to affect the results of dipole−CSA cross-correlation measurements.[44] However, another type of exchange, hindered rotation about the $C^{\delta}-N^{\epsilon 2}$ bond, can influence the results of the discussed relaxation experiments. Recent measurements[45] performed on Asn and Gln side chains of the small globular protein toxin α from *Naja nigricollis* with 61 amino acids yielded rotation rates in the range $0-1\ s^{-1}$ for side chains buried in the core of the protein and $1-10\ s^{-1}$ for more mobile side chains. The low-end exchange rates are too small to significantly affect the results of dipole−CSA cross-correlation measurements for the buried Gln 41 side chain performed with mixing times as short as 50−150 ms. However, the high-end exchange rates are large enough to cause partial averaging of the observed cross-correlations involving $H^{\epsilon 21}$ and $H^{\epsilon 22}$ in the mobile Gln 62 side chain.

The rotational correlation time for ubiquitin, $\tau_c = 5.03$ ns, has been determined from the backbone T_1 and dipole−CSA cross-correlated relaxation measurements on $^{15}N-^1H^N$. Due to the high D_2O content of the solution affecting viscosity, this value for τ_c is ∼20% larger than the one found for ubiquitin dissolved in a 95% H_2O/5% D_2O solvent.[1b,33,34]

Interpretation of Dipole−CSA Cross-Correlated Relaxation Data. In the 2D spectra resulting from the described experiment, both (isomeric) NHD groups exhibit doublets in the ω_1 dimension. The ratio of the intensities of the two doublet components yields the dipole−CSA cross-correlated relaxation rate constant Γ(N,NH). For the NH_2 groups, the intensity ratio of the peaks separated by $2J_{NH}$ corresponds to a modified cross-correlated relaxation rate constant Γ_Σ(N,NH).

The dipole−CSA cross-correlated relaxation rate constant Γ(N,NH) is given by[46]

$$\Gamma(\mathrm{N,NH}) = -\frac{1}{30}\gamma_N B_0 \xi_{NH} \sum_{k=1,2} \{4J^{kk}_{N,NH}(0) + 3J^{kk}_{N,NH}(\omega_N)\} \quad (1)$$

where B_0 is the magnetic field strength, γ_N is the gyromagnetic ratio of ^{15}N, $\xi_{NH} = (\mu_0/4\pi)(h/2\pi)\gamma_N\gamma_H\langle r_{NH}^{-3}\rangle$, and r_{NH} is the distance between spins N and H. The real parts of the cross-spectral density functions $J^{kk}_{N,NH}(\omega)$ are defined as

$$J^{kk}_{N,NH}(\omega) = \int_{-\infty}^{\infty} C^{kk}_{N,NH}(\tau)\cos(\omega\tau)\,d\tau \quad (2)$$

where $C^{kk}_{N,NH}(\tau)$ is the dipole−CSA cross-correlation function

$$C^{kk}{}_{N,NH}(\tau) = \overline{4\pi(\sigma_{kk}(t) - \sigma_{33}(t))Y_{20}(\Omega^k_N(t))Y^*_{20}(\Omega_{NH}(t+\tau))}$$

$Y_{2m}(\Omega)$ are the normalized second-order spherical harmonics, $\Omega_{NH}(t)$ specifies the orientation of the NH vector in the laboratory frame at time t, $\Omega^k_N(t)$ specifies the orientation of the CSA principal axis associated with the principal value σ_{kk} in the laboratory frame at time t, and the horizontal bar denotes a time average over t. Assuming isotropic overall tumbling and independence of internal and overall motion, one obtains

$$C^{kk}_{N,NH}(\tau) = \frac{4\pi}{5}e^{-\tau/\tau_c} \times \sum_{m=-2}^{2} \overline{(\sigma_{kk}(t) - \sigma_{33}(t))Y_{2m}(\Omega^{mol,k}_N(t))Y^*_{2m}(\Omega^{mol}{}_{NH}(t+\tau))} \quad (3)$$

where $\tau_c = (6D)^{-1}$ is the overall tumbling correlation time and D is the rotational diffusion constant. $\Omega^{mol,k}_N(t)$ and $\Omega^{mol}_{NH}(t)$ are the time-dependent principal axis directions of the CSA and dipolar tensors, respectively, in the molecular diffusion frame, which is the frame of the reoriented MD snapshots. Thus, the CSA trajectories of the previous section can be directly inserted in eq 3 in order to calculate the relaxation parameters of interest.

(42) Grzesiek, S.; Bax, A. *J. Magn. Reson.* **1992**, *96*, 432−440.
(43) Yang, D.; Mittermaier, A.; Mok, Y.-K.; Kay, L. E. *J. Mol. Biol.* **1998**, *276*, 939−954.
(44) Rama Krishna, N.; Partha Sarathy, K.; Hunag, D.-H.; Stephens, R. L.; Glickson, J. D.; Smith, C. W.; Walter, R. *J. Am. Chem. Soc.* **1982**, *104*, 5051−5053.
(45) Guenneugues, M.; Drevet, P.; Pinkasfeld, S.; Gilquin, B.; Ménez, A.; Zinn-Justin, S. *Biochemistry* **1997**, *36*, 16097−16108.
(46) Goldman, M. *J. Magn. Reson.* **1984**, *60*, 437−452.

Table 4. Experimental vs Computed Cross-Correlated Relaxation Rate Constants for Gln 41 and Gln 62 Side Chains in Ubiquitin

residue	relaxation rate const	exptl (s^{-1})	computed with eq 3[a] (s^{-1})	computed with approx eq 6[a,b] (s^{-1})
Gln 41	$\Gamma(N,NH^{\epsilon 21})$	4.8	4.12	4.17
	$\Gamma(N,NH^{\epsilon 22})$	1.6	1.65	1.61
	$\Gamma_\Sigma(N,NH)$	6.1	5.73[c]	5.76[c]
Gln 62	$\Gamma(N,NH^{\epsilon 21})$	0.4	0.024	0.025
	$\Gamma(N,NH^{\epsilon 22})$	*d*	0.357	0.354
	$\Gamma_\Sigma(N,NH)$	1.1	0.340[c]	0.337[c]

[a] The correlation functions obtained from the MD and CSA trajectories are fitted with six weighted exponentials following the approach of ref 37. In these multiexponential functions, the correlation times exceeding 10 ns are replaced by infinitely long correlation times. The overall tumbling correlation time $\tau_c = 5.03$ns is used (which is due to the high D_2O content of the used solvent higher than the one found for ubiquitin dissolved in H_2O[1,33,34]). [b] The unit vectors $\mathbf{d}(\Omega_q(t))$ forming a basis are described in the caption of Figure 4 and the constants c_q^k are determined from the average CSA orientations in this basis. [c] Including small Γ_H terms involving proton CSA (see eq 5 and the following discussion). [d] Was not measured because of spectral overlap.

The pair of NH_2 multiplet peaks with $2J_{NH}$ separation in the ω_1 dimension can be used to measure an additional cross-correlated relaxation parameter $\Gamma_\Sigma(N,NH)$. The ratio of the intensities of these two peaks decays exponentially as a function of the mixing time with the cross-correlation rate constant

$$\Gamma_\Sigma(N,NH) = \Gamma(N,NH^{\epsilon 21}) + \Gamma(N,NH^{\epsilon 22}) + \Gamma_H(H^{\epsilon 21},H^{\epsilon 21}H^{\epsilon 22}) + \Gamma_H(H^{\epsilon 22},H^{\epsilon 22}H^{\epsilon 21}) \quad (4)$$

which also contains the "proton-only" terms Γ_H:

$$\Gamma_H(H,HH') = -\frac{1}{30}\gamma_H B_0 \xi_{HH'} \sum_{k=1,2} 3J^{kk}_{H,HH'}(\omega_H) \quad (5)$$

where $\xi_{HH'}$ and $J^{kk}_{H,HH'}$ are the homonuclear analogues to ξ_{NH} and $J^{kk}_{N,NH}$ of eqs 1 and 2.

Analysis of the CSA trajectories reveals that the characteristic correlation time of the CSA tensor fluctuations is below 4 ps, which is the resolution of the CSA trajectory. Such fast motions are not relaxation-active so that for the purpose of the relaxation analysis it is sufficient to take into account an average CSA tensor that is rigidly attached to the amide plane subject to internal and overall motions. If the direction of the average CSA principal axis *k*, $\Omega^k(t)$, is expanded in terms of local unit vectors (and their pairwise cross products) $\mathbf{d}(\Omega_q^{mol}(t))$ pointing along $\Omega_q^{mol}(t)$, such that $\mathbf{d}(\Omega^k(t)) = \sum_q c_q^k\, \mathbf{d}(\Omega_q^{mol}(t))$, the correlation function $C^{kk}_{N,NH}(\omega)$ can be expressed as follows:

$$C^{kk}_{N,NH}(\tau) \approx \frac{4\pi}{5} e^{-\tau/\tau_c}(\overline{\sigma_{kk}} - \overline{\sigma_{33}}) \times \sum_{m=-2}^{2} \overline{Y_{2m}(\sum_q c_q^k\, \mathbf{d}(\Omega_q^{mol}(t)))Y^*_{2m}(\Omega_{NH}^{mol}(t+\tau))} \quad (6)$$

where $\overline{\sigma_{kk}}$ are the time-averaged CSA components.

To compare experiment and theory, the dipole−CSA cross-correlation rate constants $\Gamma(N,NH^{\epsilon 21})$, $\Gamma(N,NH^{\epsilon 22})$, and $\Gamma_\Sigma(N,NH)$ were calculated for Gln 41 and Gln 62. The correlation functions were obtained from the MD trajectory (for the dipolar part) and CSA trajectories that included the environment effects. The results for the rigorous treatment based on eq 3 as well as the treatment based on eq 6 with time-invariant CSA components are given in Table 4 together with the experimental results. The error introduced by the approximate treatment is insignificant,

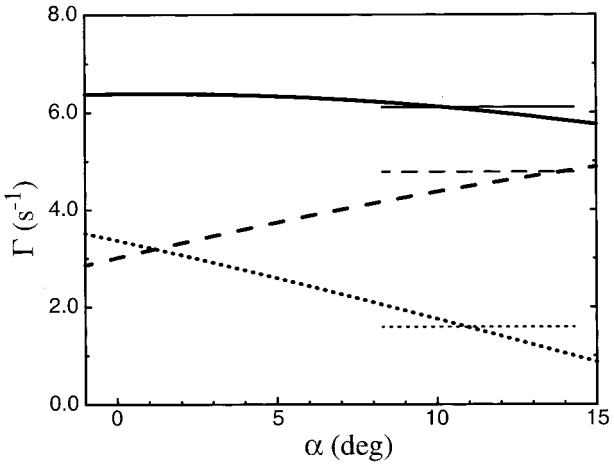

Figure 5. Dipole−CSA cross-correlated relaxation rates in Gln 41 as functions of the angle α: $\Gamma(N,NH^{\epsilon 21})$ (bold dashed line), $\Gamma(N,NH^{\epsilon 22})$ (bold dotted line), and $\Gamma_\Sigma(N,NH)$ (bold solid line). The three thin horizontal lines indicate the corresponding experimental values at 600-MHz proton frequency and 300 K. The three bold curves represent the results of the model calculations based on the MD and DFT data using the approximate eq 6. The angle α specifies the orientation of the *x* principal axis of the $N^{\epsilon 2}$ CSA tensor, which is assumed to lie in the amide plane with respect to the NC^δ bond (see text). The CSA principal values from Table 3 (Gln 41 with environment) have been used. The distances $NH^{\epsilon 21}$ and $NH^{\epsilon 22}$ are set to 1.02 Å. The Γ_H contributions to $\Gamma_\Sigma(N,NH)$ have been ignored (see text).

indicating that the time variation of the CSA tensor relative to the molecular frame is not relaxation-active.

For the evaluation of $\Gamma_\Sigma(N,NH)$, the contributions from $\Gamma_H(H^{\epsilon 21},H^{\epsilon 21}H^{\epsilon 22})$ and $\Gamma_H(H^{\epsilon 22},H^{\epsilon 22}H^{\epsilon 21})$ of eq 5 were computed in an analogous way using proton CSA tensors taken either from solid-state NMR measurements[47] or from the DFT computations. Very minor contributions were obtained, e.g., for Gln 41, $\Gamma_H(H^{\epsilon 21},H^{\epsilon 21}H^{\epsilon 22}) \cong -0.01\ s^{-1}$ and $\Gamma_H(H^{\epsilon 22},H^{\epsilon 22}H^{\epsilon 21}) \cong -0.04\ s^{-1}$. If these $\Gamma_H(H,HH')$ terms can be neglected, the rate constant Γ_Σ is, according to eq 4, equal to the sum of the two cross-correlated relaxation terms $\Gamma(N,NH^{\epsilon 21})$ and $\Gamma(N,NH^{\epsilon 22})$ of eq 1. Γ_Σ depends less on the CSA tensor orientation than either of the two $\Gamma(N,NH)$ terms.

The sensitivity of the cross-correlation data with respect to the average orientation of the $N^{\epsilon 2}$ CSA tensor relative to the amide plane was investigated for Gln 41. In the following, it is assumed that the *x* and *z* principal axes of the ^{15}N CSA lie in the carboxamide plane (i.e., angle β is set to zero; cf. Table 3) and that the angle α between the *x* axis and the $N^{\epsilon 2}C^\delta$ bond is constant. The CSA orientations, $\Omega^k(t)$, can then be determined from the internuclear vectors $N^{\epsilon 2}C^\delta(t)$, $N^{\epsilon 2}H^{\epsilon 21}(t)$, and $N^{\epsilon 2}H^{\epsilon 22}(t)$ extracted from the MD trajectory. The results are inserted in eq 6 and the dipolar-CSA relaxation rate constants are computed for different values of angle α (see Figure 5). Comparison with the experimental relaxation data supports the value for the angle α obtained by the DFT calculations of Table 1.

The theoretical curves plotted in Figure 5 rely on MD and MD/DFT CSA data. To further test the consistency between MD/DFT computations and the experiment, $^{15}N^{\epsilon 2}$ T_1 relaxation times and saturation-transfer NOEs were measured and computed. Experimental T_1^{-1} values of 2.4 and 2.3 s^{-1} for the $N^{\epsilon 2}H^{\epsilon 21}D^{\epsilon 22}$ and $N^{\epsilon 2}D^{\epsilon 21}H^{\epsilon 22}$ isotopomers are in the same range as the calculated values of 1.9 and 2.0 s^{-1}. The calculated results

(47) Gerald, R., II; Bernhard, T.; Haeberlen, U.; Rendell, J.; Opella, S. *J. Am. Chem. Soc.* **1993**, *115*, 777−782. Wu, C. H.; Ramamoorthy, A.; Gierasch, L. M.; Opella, S. J. *J. Am. Chem. Soc.* **1995**, *117*, 6148−6149.

include dipolar and CSA autorelaxation rates obtained by a computational procedure similar to the one used for the cross-correlation rate constants. Measured NOE values of 0.86 and 0.82 are in fair agreement with the calculated parameters of 0.71 and 0.79, respectively.

For Gln 62, an analysis analogous to the one shown in Figure 5 has not been performed, since the experimental data on Gln 62 are incomplete and the measurements of the weak cross-correlation effects in the presence of fast transverse relaxation are less accurate than in case of Gln 41 (Table 4). While the experimental data indicate that the side chain of Gln 62 is highly mobile, which is in qualitative agreement with the MD simulation, a detailed description of its internal motion is not possible on the basis of the existing experimental data. It has been suggested in the literature[48] that fast χ_3 motion leads to distinctly different dynamics for the $NH^{\epsilon 21}$ and $NH^{\epsilon 22}$ vectors (see Figure 3). We were unable to observe this effect experimentally, which may be in part due to chemical exchange that can be sufficiently fast for mobile side chains (see Experimental Information) to cause averaging and equalization of the $\Gamma(N,NH^{\epsilon 21})$ and $\Gamma(N,NH^{\epsilon 22})$ rate constants.

Relaxation by the Antisymmetric CSA Tensor. The antisymmetric part ϱ^{anti} of the $N^{\epsilon 2}$ CSA tensor for computing relaxation rate constants was not considered so far. Since this part of the CSA interaction is nonsecular with respect to the Zeeman interaction, it is not manifested in standard solid-state NMR experiments. The data extracted from the computed CSA trajectories, including the environment, yield the average values $\bar{\sigma}_{12} = -2.3$ ppm, $\bar{\sigma}_{13} = 21.3$ ppm, and $\bar{\sigma}_{23} = -0.2$ ppm for Gln 41 and $\bar{\sigma}_{12} = -0.4$ ppm, $\bar{\sigma}_{13} = 21.1$ ppm, and $\bar{\sigma}_{23} = -0.6$ ppm for Gln 62 in the principal axes system of ϱ^{sym}. As is well-known, the antisymmetric part of the CSA tensor, which transforms as a rank 1 tensor under rotations in real space, does not affect the cross-correlation rates of the dipolar and symmetric CSA interactions which are of rank 2. Its contribution to the ^{15}N longitudinal autorelaxation rate is known to be given by[49]

$$T_{1,\mathrm{asym}}^{-1}(\mathrm{N}) = \frac{1}{3}\gamma_N^2 B_0^2\{\bar{\sigma}_{23}^2 j_N^{11}(\omega_N) + \bar{\sigma}_{13}^2 j_N^{22}(\omega_N) + \bar{\sigma}_{12}^2 j_N^{33}(\omega_N) + 2\bar{\sigma}_{12}\bar{\sigma}_{23} j_N^{13}(\omega_N) + 2\bar{\sigma}_{23}\bar{\sigma}_{13} j_N^{12}(\omega_N) + 2\bar{\sigma}_{12}\bar{\sigma}_{13} j_N^{23}(\omega_N)\} \quad (7)$$

where the power spectral densities corresponding to the first-rank correlation functions can be expressed through the time-dependent orientations of the CSA principal axes:

$$j_N^{kl}(\omega) = \frac{4\pi}{3}\int_{-\infty}^{\infty} e^{-\tau/3\tau_c} \times \sum_{m=-1}^{1} \overline{Y_{1m}(\Omega_N^{\mathrm{mol},k}(t)) Y_{1m}^*(\Omega_N^{\mathrm{mol},l}(t+\tau))} \cos(\omega\tau)\, d\tau \quad (8)$$

$\Omega_N^{\mathrm{mol},k}$ is the orientation of the CSA principal axis k in the frame of the reoriented MD snapshots (molecular diffusion frame). The terms $j_N^{kl}(\omega)$ with $k \neq l$ of eq 7 are very small, also because the corresponding correlation functions start at zero for $\tau = 0$. Thus, $T_{1,\mathrm{asym}}^{-1}$ is dominated by the terms with $k = l$. Computations based on eq 7 indicate that the antisymmetric CSA contribution to $T_{1:\mathrm{asym}}^{-1}(\mathrm{N})$ is 4% of its symmetric counterpart in the case of Gln 41 and 2% in the case of Gln 62. These results are similar to recent estimates given for ^{15}N relaxation of formamide extrapolated to the slow-tumbling regime.[50]

5. Conclusion

Recent progress in NMR methodology for the determination of a variety of auto- and cross-correlated relaxation parameters gives new possibilities to test detailed motional models for their consistency. A prerequisite for such investigations is the accurate knowledge of the principal axes and principal values of the relevant nuclear interactions. In this work, we have shown that the traditional method, where such information is retrieved by solid-state NMR of model systems, can be usefully complemented or even substituted by DFT calculations applied to an MD trajectory of the actual system under investigation. Hydrogen bonding and electrostatic interactions can have a significant influence on the ^{15}N CSA tensors, as was demonstrated by DFT calculations on crystalline Asn and the AlaAla dipeptide. Motional averaging as present in the MD simulation of ubiquitin, however, may reduce the effects of hydrogen bonding on CSA tensors since for much of the time the hydrogen bond may be far from ideal. As a consequence, the time-averaged CSA tensors of $^{15}N^{\epsilon 2}$ in Gln 41 and Gln 62 computed using DFT are similar despite their different chemical environments. The DFT calculations agree with the dipole−CSA cross-correlated relaxation data of the $N^{\epsilon 2}H^{\epsilon 21}D^{\epsilon 22}$ and $N^{\epsilon 2}D^{\epsilon 21}H^{\epsilon 22}$ side-chain groups that are sensitive to the CSA tensor magnitudes and orientations.

The use of density functional theory for the computation of the time-dependent ^{15}N CSA tensors along an MD trajectory may further enhance the insight gained from NMR relaxation experiments on protein dynamics. Dipole−CSA cross-correlated relaxation experiments, which are sensitive to the changes in CSA tensors and can relate these changes to structural parameters, will particularly benefit from this additional source of information. DFT calculations are expected to become also increasingly useful for structural solid-state NMR studies where the knowledge of the orientation of the CSA tensor in a molecular frame is a prerequisite for the determination of molecular structures.[51]

Acknowledgment. The authors thank Dr. Hongbiao Le for stimulating discussion and Dr. Bernhard Brutscher for implementing the 3D relaxation experiment of section 4. Prof. V. Malkin and Dr. M. Kaupp supported the project with helpful discussions and advice concerning the use of deMon. N.R.S. is a recipient of NSERC scholarship (Canada). This work was supported by the Swiss National Science Foundation.

Supporting Information Available: Five tables (corrected fractional coordinates for crystalline AlaAla; hydrogen bonds connecting atoms of the amide group of crystalline Asn to neighboring molecules; hydrogen bonds connecting atoms of the peptide group of crystalline AlaAla to neighboring molecules; polar coordinates of the CSA principal axes of AlaAla; assignment of amide resonances of Asn and Gln side chains in ubiquitin) and five figures (autocorrelation functions of dipolar $N^{\epsilon 2}-H^{\epsilon 21}$ and $N^{\epsilon 2}-H^{\epsilon 22}$ interactions calculated from MD trajectory of ubiquitin; calculated dipole−CSA cross-correlation functions for $N^{\epsilon 2}$ CSA and $N^{\epsilon 2}-H^{\epsilon 2k}$ ($k = 1$ or 2) dipole interactions; calculated scatterplots of χ_3 vs χ_2 for Gln 41 and Gln 62; NMR pulse sequence for the 3D CT-HSQC experiment; selected cross sections of the 3D CT-HSQC spectrum) (PDF). This material is available free of charge via the Internet at http://pubs.acs.org.

JA984159B

(48) Pervushin, K.; Wider, G.; Wüthrich, K. *J. Am. Chem. Soc.* **1997**, *119*, 3842−3843.

(49) Spiess, H. W. In *NMR Basic Principles and Progress*; Diehl, P., Fluck, E., Kosfeld, E., Eds.; Springer: Berlin, 1978; Vol. 15, p 55.

(50) Kowalewski, J.; Werbelow, L. *J. Magn. Reson.* **1997**, *128*, 144−148.

(51) Robyr, R.; Utz, M.; Gan, Z.; Scheurer, C.; Tomaselli, M.; Suter, U. W.; Ernst, R. R. *Macromolecules* **1998**, *31*, 5818−5822.